Journal of Alloys and Compounds 509 (2011) 4047–4052

Contents lists available at ScienceDirect

Journal of Alloys and Compounds

journal homepage: www.elsevier.com/locate/jallcom

Optical properties of highly Er^{3+}-doped sodium–aluminium–phosphate glasses for broadband 1.5 μm emission

A. Amarnath Reddy[a], S. Surendra Babu[b], K. Pradeesh[a], C.J. Otton[c], G. Vijaya Prakash[a,*]

[a] Nanophotonics Laboratory, Department of Physics, Indian Institute of Technology Delhi, Hauz Khas, New Delhi 110016, India
[b] Laser Instrumentation Design Centre, Instrument Research and Development Establishment, Dehradun 248008, India
[c] Valencia Nanophotonics Technology Center, Universidad Politécnica de Valencia, 46022 Valencia, Spain

ARTICLE INFO

Article history:
Received 23 September 2010
Received in revised form 3 January 2011
Accepted 3 January 2011
Available online 6 January 2011

Keywords:
Er-doped glass
Optical spectroscopy
Broadband
Gain cross-section

ABSTRACT

Erbium-doped $Na_3Al_2P_3O_{12}$ (NAP) glasses with compositions 92NAP–(8−x)Al_2O_3–(x)Er_2O_3 (where x = 2–8) were prepared and characterized for absorption, visible and NIR emission and decay time properties. Judd–Ofelt analysis has been carried out to predict radiative properties of luminescent levels of Er^{3+} ions. Comparatively larger photoluminescence lifetimes (7.86 ms) and larger quantum efficiencies (74%) for the laser transition, $^4I_{13/2} \rightarrow {}^4I_{15/2}$ (at 1.54 μm) are observed. The moisture insensitivity, large Er^{3+} ion doping capability and relatively high-gain and broad emission at 1.5 μm are the most notable features of these glasses to realize efficient short-length optical amplifiers.

1. Introduction

Rapid technological growth in the fields of telecommunication and data transfer has kept in phase with the development of optical amplification based on the rare earth (RE) doped fiber amplifiers. Particularly, Er^{3+} and/or Tm^{3+} ion doped fibers make it possible to amplify optical signals in the range of C-band, 1530–1565 nm or S-band, 1460–1530 nm. Though single or co-doped RE based glass fibers/waveguides are of great promise, the focus has been concentrated mostly on silicate glasses although their amplified spontaneous emission (ASE) bandwidths are limited to few tens of nanometers (~40 nm). Rare earth co-doped fluoride and tellurite glasses have shown ASE with considerably extended bandwidth, where the emission broadness arises due to inter-ion energy transfer. By and large, the suitability of rare earth doping and the proper choice of glass matrix are still unclear [1–5].

Recently, phosphate glasses have received a great deal of attention due to their potential application in optical data transmission, detection, sensing and laser technology, waveguide and fiber optical amplifier devices [6–8]. In general, the RE emission in glassy matrix is strongly dependent on crystal field effects, local environment where the ion is situated, phonon energies, refractive index and precise details about defect energy levels (Urbach tails) extended into the band gap. Compared to silica glasses, phosphate glasses offer distinct optical properties such as large infrared transmission window, good chemical durability, high gain density, wide bandwidth emission spectrum and low up-conversion characteristics. The high gain density in phosphate glass is due to high solubility of active ions introduced into a relatively small volume [9–13]. Introducing Al_2O_3 into phosphate glass network increases the cross-links between PO_4 tetrahedral in the glass which results in an increase in the aqueous durability and glass transition temperature, and a decrease in thermal expansion coefficient [14]. The addition of Na_2O further improves the RE solubility leading to the possibility of using a high concentration of dopants [15]. Also the presence of Na_2O in the glass provides the suitability for the fabrication of optical wave guide devices by ion exchange method [16].

The present paper deals with the absorption and emission properties of erbium doped sodium super ionic conductor (NASICON) type [9,11,12,17] Sodium–aluminium–phosphate (NAP) glass systems. Absorption spectral intensities of varied Er^{3+} concentration in NAP glasses are analyzed by using Judd–Ofelt theory. A detailed study of visible and near infrared photoluminescence properties has been carried out. The results are examined with respect to the concentration effects, and are compared with the other reported glass systems.

2. Experimental procedure

Er^{3+}-doped $Na_3Al_2P_3O_{12}$ (NAP) glasses in the form of 92NAP–(8−x)Al_2O_3–(x)Er_2O_3 (where x = 2–8) were prepared by the conven-

* Corresponding author. Tel.: +91 011 2659 1326; fax: +91 011 2658 1114.
E-mail addresses: prakash@physics.iitd.ac.in, gaddam.vijaya.prakash@gmail.com (G. Vijaya Prakash).

0925-8388/$ – see front matter © 2011 Elsevier B.V. All rights reserved.
doi:10.1016/j.jallcom.2011.01.016

Table 1
Physical and optical properties of Er^{3+} doped NAP glasses.

Property	NAP	NAP:Er^{3+}						
		2 wt%	3 wt%	4 wt%	5 wt%	6 wt%	7 wt%	8 wt%
E_{opt} (eV)	2.97	3.32	3.31	3.30	3.31	3.34	3.35	3.39
Urbach, ΔE (eV)	0.24	0.33	0.34	0.36	0.37	0.31	0.24	0.18
Refractive index (n)	1.52	1.53	1.55	1.55	1.58	1.59	1.61	1.62
Density, ρ (g/cm^3)	2.56	2.53	2.54	2.56	2.59	2.604	2.609	2.66
Molecular weight, M (g/mol)	407.85	334.26	335.32	335.51	336.15	336.45	336.98	337.37
Molar volume, V_m (cm^3/mol)	159.31	132.11	132.02	131.05	129.79	129.40	129.11	126.83
Molar refraction, R_m (cm^3/mol)	48.35	40.61	42.00	42.00	43.31	43.61	44.76	44.61
Reflection loss (%)	4.24	4.35	4.64	4.70	5.08	5.17	5.46	5.61
Polarisability, α (A^3)	19.17	16.10	16.66	16.66	17.17	17.29	17.75	17.69

tional melting procedure [10]. Stoichiometric amounts of $(NH_4)_2HPO_4$, Al_2O_3 and $NaNO_3$ (analytical grade) were mixed with required wt% of Er_2O_3 (Aldrich Chemical Co., USA) and were taken in an agate mortar and grounded thoroughly using spectroscopic grade proponal. Then the mixer was taken into a silica crucible and placed in an electric furnace. The temperature was raised slowly to 300 °C and was maintained for about an hour and then increased up to 600 °C to ensure a complete decomposition of $(NH_4)_2HPO_4$ into P_2O_5. Subsequently the temperature of the mixture was raised to 1250 °C to get a clear melt. The homogeneity of the product was ensured by repeated stirring of the melt. The bubble free and homogeneous melt was poured on a preheated brass mould and were annealed at 350 °C for 24 h and then allowed to cool slowly to room temperature. The glass samples were polished for the optical measurements.

The absorption spectra of Er^{3+}-doped NAP glasses were recorded using a PerkinElmer UV–vis–NIR spectrophotometer with a spectral resolution of 0.01 nm. 532 nm of DPSS laser and 975 nm of a diode laser were used as excitation sources for both luminescence emission and decay time measurements in visible and near infrared region, respectively, and recorded with a monochromator (Acton SP2300), attached to PMT and InGaAs detectors with a spectral resolution of 0.1 nm. Decay curves were obtained, with resolution of 0.001 ms, using a digital storage oscilloscope (Tektronix TDS1001B) coupled to PMT of the monochromator. Refractive index measurements for glasses were carried out by Brewster angle setup consisting of He–Ne laser (632 nm) and a Si-detector.

3. Results and discussion

The intra 4*f* transitions of Er^{3+} ions from $^4I_{13/2} \rightarrow {}^4I_{15/2}$ transition corresponding to an emission at 1530 nm, is very important in the fields of laser material and optical communications. As the output power of the lasers and gain of the short-length optical amplifiers strongly depends on the concentration of Er^{3+} ion in a given host material, in the present work optical and physical properties of high Er^{3+} ion doped NAP glasses are extensively explored.

3.1. Physical and structural properties

The physical and optical parameters such as refractive index (η), density (ρ), molar refractive index (R_m), molar volume (V_m), optical band gap (E_{Opt}) and Urbach energies (ΔE) of un-doped and Er^{3+}-doped NAP glasses (for various Er_2O_3 concentrations) were determined from various experiments and are reported in Table 1. These glasses, in general, are moisture insensitive, compatible for ion-exchange waveguide fabrication and capable of accepting large concentration of RE ions (up to 8 wt% or $\sim 8 \times 10^{20}$ ions/cm^3) without losing the transparency. Estimated optical band gap values, from the absorption spectra, of the NAP glasses are in the ranges 2.97–3.39 eV. The widths of localized states within the optical band gap, known as Urbach energies (ΔE), were also estimated from the absorption spectra and the range of the values are found to be 0.18–0.37 eV, which are as close to those values reported for other phosphate glasses [18,19]. Such lower values suggest minimum defects, leading to long-range order in the present glass systems. Refractive index values of Er^{3+} ion doped NAP glasses show increasing trend with the increase of Er^{3+} ion content. Generally in oxide glasses, the ionic refractivity of non-bridging oxygens is larger than the ionic refractivity of bridging oxygens [20]. According to the crystalline data for another alkali ion based crystalline NASICON, $K_3Al_2P_3O_{12}$ [17], comparable to the present NAP glass, the structure could be visualized as anionic framework built from corner-shared AlO_4 and PO_4 tetrahedral coordination, where phosphate tetrahedra pointing their unshared oxygen atoms towards the channels occupied by alkali ions. Therefore, this type of structure could possibly increase number of non-bridging oxygen, when Al^{3+} was compensated with the Er^{3+}, which could be one of the possible reasons for increase in refractive index values [21].

Fig. 1 shows the FTIR spectra of NAP glass along with peak assignments [12,13,22,23]. As seen from the figure, broad and strong band around 1076 cm^{-1} is indicative of the PO_4 symmetric stretching vibrations (Q^1) band in the present system [13]. Other peaks could be assigned to the deformation mode of PO^- group at 529 cm^{-1}, the P–O–P group symmetric stretching vibration band at 729 cm^{-1} [22,23]. The bands at 1645 and 3429 cm^{-1} are traced to the free H_2O molecules and OH^- stretching vibration modes, respectively [12].

3.2. Absorption spectra and Judd–Ofelt analysis

The absorption spectra of various wt% of Er_2O_3 doped NAP glasses, consists of absorption bands corresponding to the absorptions from the ground state $^4I_{15/2}$ of Er^{3+} ions (Fig. 2). In general, the spectral lines show inhomogeneous broadening as the degeneracy of levels is not completely removed, which is a consequence of the absence of long-range order in the glass host producing changes in the micro symmetry around the Er^{3+} ions. The linear variation of integrated absorption as a function of Er^{3+} ion concentration in NAP glass (inset of Fig. 2), indicates the presence of homogeneously distributed similar local structure around the Er^{3+} ions, even at higher concentrations.

From the absorption spectra, experimental oscillator strengths (f_{exp}) of the transitions originating from $^4I_{15/2}$ were obtained and are used in the Judd–Ofelt analysis [24,25]. The three Judd–Ofelt

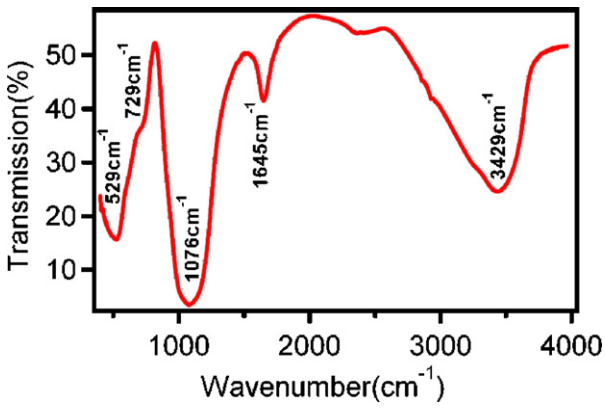

Fig. 1. FTIR spectra of NAP glass.

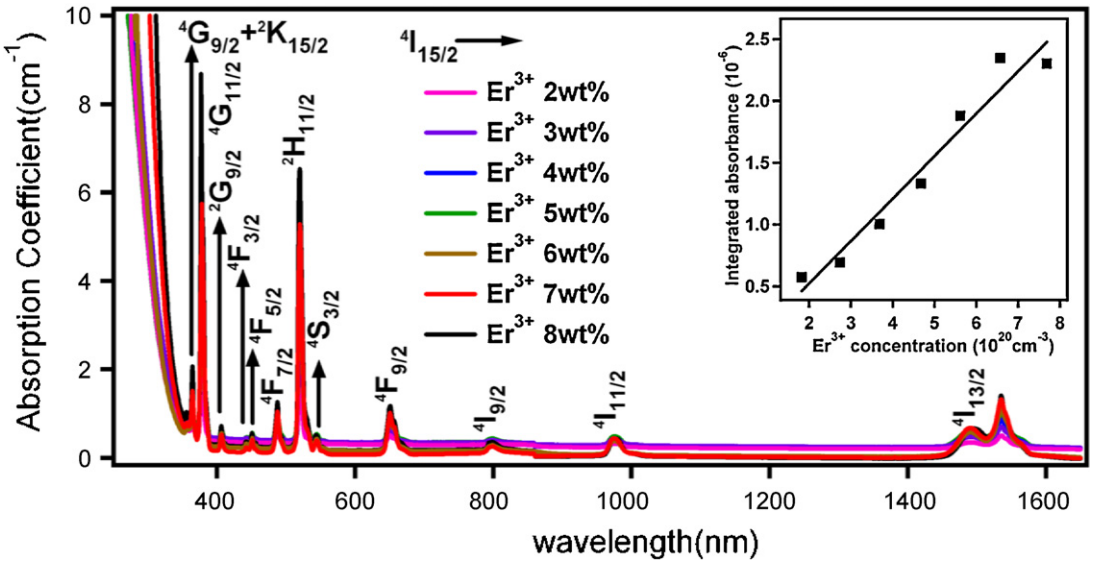

Fig. 2. Absorption spectra of Er^{3+}-doped NAP glasses for various Er^{3+} ion concentrations. Inset shows variation of integrated absorption with respect to Er^{3+} ion concentration.

parameters (Ω_λ, $\lambda = 2, 4$ and 6), were calculated by fitting the experimental oscillator strengths to the calculated oscillator strengths as described in our earlier report [10] and are collected in Table 2 along with other reported Er^{3+}-doped phosphate [10,26] tellurite [27] and fluoride [28] glasses. In the present glass, the Ω_2 parameter is in decreasing trend with increasing Er^{3+} concentration up to 5 wt% and later shows increasing trend (Table 2). In general, the observed Ω_2 values are close to that of the covalent glasses like phosphates and tellurites and slight higher than that of the ionic glasses like fluorides [10,26–28]. Generally, it is believed that both covalence and site selectivity of RE ion with non-centro symmetric potential contribute significantly to Ω_2, while other parameters Ω_4 and Ω_6 are mostly dependent on bulk properties [26,29,30]. Also, Ω_2 is strongly dependent on the hypersensitive transitions. Hypersensitivity is related to the covalency through nephelauxetic effect and affects the polarizability of the ligands around the rare earth ions. Higher ligand polarizability results in a larger overlap between rare earth ions and ligands orbital, i.e., higher degree of covalency between rare earth ions and the ligands. Thus, the increment of the rare earth ions concentration (with reduction of Al^{3+} content) decreases the Ω_2 and the degree of covalency. However, in the present case, lower than 5 wt% Er^{3+} doping is predominantly due to the environment effects around Al^{3+} ions, and above is dominated by the covalancy parameter [31].

3.3. Visible and NIR photoluminescence properties

Visible and near-infrared photoluminescence (PL) spectra of Er^{3+}-doped NAP glasses are recorded using 532 nm and 975 nm lasers, respectively (Fig. 3). The visible PL of these glasses exhibit bright green PL (545 nm) corresponding to $^4S_{3/2} \rightarrow {}^4I_{15/2}$ transition with other weak peaks at around 650 nm and 850 nm due to $^4F_{9/2} \rightarrow {}^4I_{15/2}$ and $^4I_{9/2} \rightarrow {}^4I_{15/2}$ transitions. The near-infrared PL spectra recorded using 975 nm excitation shows strong peak at 1534 nm due to $^4I_{13/2} \rightarrow {}^4I_{15/2}$ transition, with no traces of visible upconversion PL even at 1 W pump powers. While the intensity of $^4S_{3/2}$ (545 nm) emission is increasing linearly with increase in Er^{3+} ion concentration, the intensity of $^4I_{13/2}$ (1530 nm) increases with increase in Er^{3+} ion concentration up to 7 wt% and drastically decreased for 8 wt% glass (Fig. 4).

The transient PL behavior of both $^4S_{3/2}$ and $^4I_{13/2}$ transitions for various Er^{3+} ion concentrations are measured and are shown in Fig. 5. It is interesting to note that the PL decay of $^4S_{3/2}$ level is found to be single exponential for all the studied concentrations of Er^{3+} ions. Moreover the measured lifetime of $^4S_{3/2}$ level is of 0.49 ms and mostly insensitive to the increasing concentration of Er^{3+} ion. Whereas, the PL decay for $^4I_{13/2}$ transition is found to be a single exponential up to 4 wt% and turned into a bi-exponential function for higher Er^{3+} concentrations (Fig. 5). From these decay curves,

Table 2
Judd–Ofelt parameters of Er^{3+} doped glasses.

Glass	Er^{3+} ion concentration, N_{Er} ($\times 10^{20}$ cm^{-3})	Ω_2 ($\times 10^{-20}$ cm^2)	Ω_4 ($\times 10^{-20}$ cm^2)	Ω_6 ($\times 10^{-20}$ cm^2)
Er:NAP (2 wt%)	1.82	3.26	0.57	0.55
Er:NAP (3 wt%)	2.74	3.25	0.54	0.55
Er:NAP (4 wt%)	3.68	3.01	0.51	0.56
Er:NAP (5 wt%)	4.67	2.97	0.49	0.54
Er:NAP (6 wt%)	5.62	2.99	0.84	0.59
Er:NAP (7 wt%)	6.57	3.24	0.80	0.71
Er:NAP (8 wt%)	7.69	3.53	0.76	0.56
Phosphate [10]	1.40	3.79	0.13	1.21
Phosphate [26]	2 mol%[a]	4.05	0.97	0.94
Phosphate [33]	1.60	6.28	1.03	1.39
Phosphate [35]	1 mol%[a]	8.05	1.46	2.28
Tellurite [27]	0.72	3.40	1.00	0.20
Fluoride [28]	1 mol%[a]	2.91	1.78	1.00

[a] Concentration in ions/cm^3 is not available.

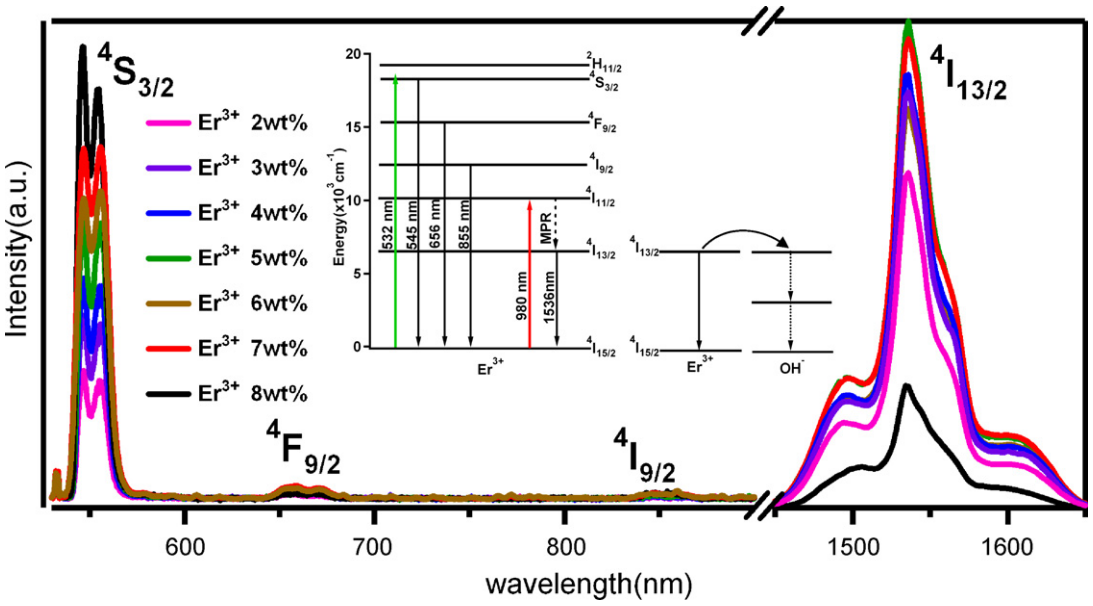

Fig. 3. Visible and near infrared PL excited with 532 nm and 980 nm laser respectively. Inset shows schematic partial energy level diagram of Er^{3+} ion doped in glass.

the effective decay times (τ_{eff}), which is considered as experimental lifetime (τ_{exp}) have been determined by using the following expression [32] $\tau_{exp} = \tau_{eff} = \int tI(t)dt / \int I(t)dt$. The obtained lifetime (τ_{exp}) values are also presented in Table 3.

For comparison, the $^4I_{13/2}$ PL life times up to 7 wt%, are comparable to other phosphate glasses doped with much less Er^{3+} concentration [10,26] but considerably more than lead based phosphate (2.75 ms), niobium based phosphate (5.4 ms) and multicomponent phosphate [32–35] and tellurite (4.1 ms) [27] glasses. In general, the lifetime of $^4I_{13/2}$ level of Er^{3+} ion is strongly governed by radiative and non-radiative processes. These experimental life times are significantly lower than the radiative lifetime (τ_{rad}) obtained from Judd–Ofelt analysis, but do not follow the trend (Table 3). This observation along with the non-exponential nature of the decay at higher concentration reveals the fact that the relaxation from $^4I_{13/2}$ level involves a combination of radiative and non-radiative de-excitation channels. Our experimental results further indicate that the process of concentration-quenching is low even up to 7 wt% in the present NAP glasses.

Quantum efficiency (η) of the $^4I_{13/2}$ level can be estimated by the relation, $\eta = (\tau_{exp}/\tau_{rad}) \times 100$ and are collected in Table 3. The variation of η along with life times with Er^{3+} ion concentration is shown in Fig. 4. These η are slightly lower than those obtained for other commercial phosphate glass (Kigre. Inc., $\eta = 80\%$) [33]. The decrease in lifetimes and η with increasing Er^{3+} ion concentration (Fig. 4B) are mostly due to the increase of energy transfer between neighborhood Er^{3+} ions and energy transfer from Er^{3+} ions to quenching centers like OH^- groups [26,36]. Specially, the free OH^- groups in the glass are regarded as effective quenchers of the IR radiation in Er^{3+}-doped phosphate glasses [37]. The energy difference between $^4I_{13/2}$ and $^4I_{15/2}$ levels Er^{3+} ions (~6500 cm^{-1}) and the OH^- vibrational frequency is about 3429 cm^{-1} in the NAP glass (FTIR spectra,

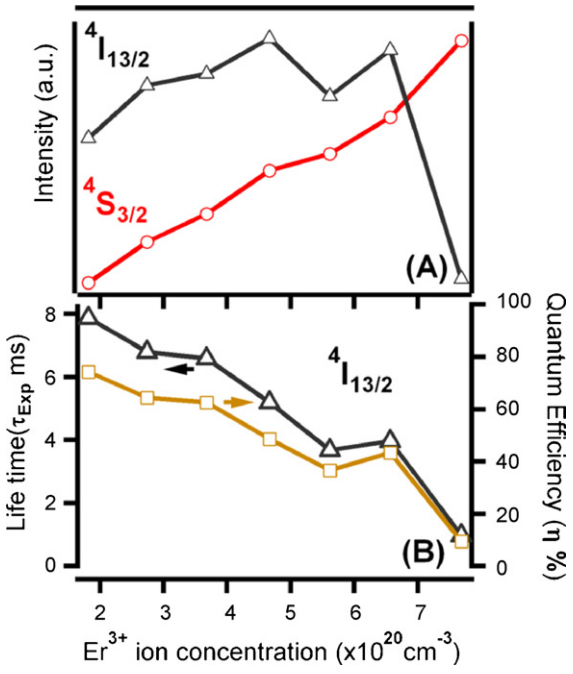

Fig. 4. (A) Variation of normalized integrated PL intensities from $^4S_{3/2}$ and $^4I_{13/2}$ to ground state $^4I_{15/2}$ transitions with respect to various Er^{3+} ion concentrations in NAP glass and (B) a plot of life time (left) and quantum efficiencies (right) of $^4I_{13/2} \rightarrow {}^4I_{15/2}$ transition for various Er^{3+} concentrations in NAP glass.

Table 3
Experimental and theoretical lifetimes (τ, ms) and quantum efficiencies (η, %) of $^4I_{13/2} \rightarrow {}^4I_{15/2}$ transition of various Er^{3+} doped glasses.

Glass	$^4I_{13/2} \rightarrow {}^4I_{15/2}$ lifetimes (ms)		Quantum efficiency, η (%)
	τ_{exp}	τ_{cal}	
Er:NAP (2 wt%)	7.86	10.57	74
Er:NAP (3 wt%)	6.80	10.55	64
Er:NAP (4 wt%)	6.59	10.52	62
Er:NAP (5 wt%)	5.20	10.71	48
Er:NAP (6 wt%)	3.68	10.04	36
Er:NAP (7 wt%)	3.97	9.16	43
Er:NAP (8 wt%)	0.97	10.28	09
Phosphate [10]	2.50	–	–
Phosphate [26]	3.16	13.80	23
Phosphate [33]	2.40	5.40	45
Phosponiobate [34]	8.00	9.96	80
Metaphosphate [35]	1.05	4.82	22
Tellurite [27]	4.10	7.90	52

Table 4
Effective line width, $\Delta\lambda_{eff}$ (nm), emission cross-section, $\sigma(\lambda_p)$ (cm^2), gain bandwidth, ΔG (cm^3) and gain per unit length, G (cm^2 s) of $^4I_{13/2} \rightarrow {}^4I_{15/2}$ transition of various Er^{3+} doped glasses.

Glass	$\Delta\lambda_{eff}$ (nm)	$\sigma(\lambda_p)$ ($\times 10^{-21}$ cm^2)	ΔG ($\times 10^{-28}$ cm^3)	G ($\times 10^{-24}$ cm^2 s)
Er:NAP (2 wt%)	52	5.58	292	43.85
Er:NAP (3 wt%)	53	5.50	293	37.40
Er:NAP (4 wt%)	54	5.33	290	35.12
Er:NAP (5 wt%)	55	5.00	275	26.00
Er:NAP (6 wt%)	57	5.07	291	18.65
Er:NAP (7 wt%)	57	5.48	311	21.75
Er:NAP (8 wt%)	56	4.87	274	04.72
Phosphate [32]	37	6.40	237	05.69
Silicate [32]	40	5.50	220	30.14
Phosphate [32]	55	8.00	440	63.20
Metaphosphate [35]	61	7.90	482	08.92
Germanate [40]	53	5.68	301	39.76
Tellurite [32]	60	6.60	396	26.40
Bismuth borate [40]	75	7.03	527	06.39

Fig. 1). Hence only two phonons are required for non-radiative de-excitation of the infrared radiation from $^4I_{13/2}$ of Er^{3+} ions as shown in the inset of Fig. 3.

To provide a comprehensive evaluation of the emission properties of the Er^{3+} ion doped NAP glasses, we have estimated important parameters those are relevant for optical amplifiers for $^4I_{13/2} \rightarrow {}^4I_{15/2}$ transition [38]. The stimulated emission cross-section, is obtained using the relation [39], $\sigma(\lambda_p) = \lambda_p^4 \tau_{rad} / 8\pi c n^2 \Delta\lambda_{eff}$, where n is the refractive index, λ_p is the emission peak wavelength, τ_{rad} is the radiative life time, $\Delta\lambda_{eff}$ is the emission effective bandwidth defined as $\Delta\lambda_{eff} = 1/I_p \int I(\lambda) d\lambda$. The gain bandwidth ($\Delta G$) is defined as product of $\Delta\lambda_{eff}$ and $\sigma(\lambda_p)$, where as the gain per unit length (G) is given by $\tau_{exp} \times \sigma(\lambda_p)$ [32]. All these optical amplifier parameters are estimated and given in Table 4. The gain bandwidths for all Er^{3+}-doped NAP glasses are found to be higher than silicate [32,40], phosphate [32,40], but lower than bismuth borate, metaphosphate [40,35] and comparable to germinate [32] glasses. Similarly, the gain per unit length is higher than those of the reported glasses (Table 4) and hence Er^{3+}-doped NAP glasses are of potential use in short-length optical amplifiers such as waveguides.

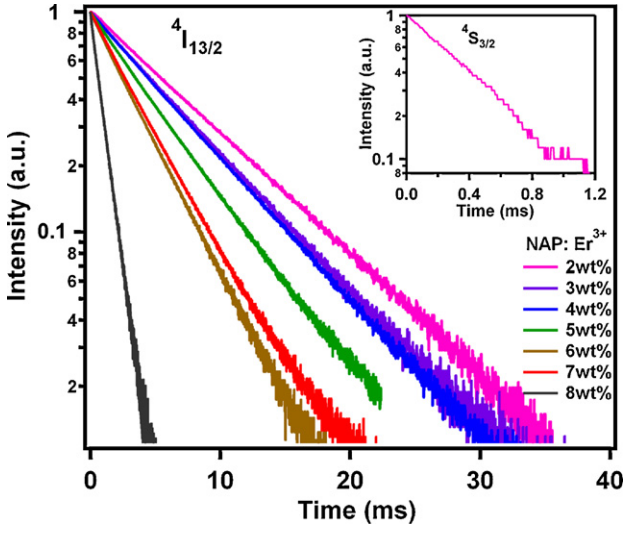

Fig. 5. PL decay curves of $^4I_{13/2} \rightarrow {}^4I_{15/2}$ transition in Er^{3+}-doped NAP glasses. Inset shows the representative luminescence decay curve of $^4S_{3/2} \rightarrow {}^4I_{15/2}$ transition of 2 wt% Er^{3+} ion doped in NAP glass.

4. Conclusions

In conclusion, optical and physical properties of a highly erbium doped sodium–aluminium–phosphate glass were presented. Optical properties, viz., optical bandgap, Urbach energies and refractive index studies show a strong correlation to the structural rearrangement of Er^{3+} ion in phosphate network. The absorption spectra are analyzed using Judd–Ofelt theory to predict the radiative properties of luminescent levels of Er^{3+} ions. The experimental lifetime (7.86 ms), quantum efficiency (74%) and other estimated stimulated emission parameters of laser transition, $^4I_{13/2} \rightarrow {}^4I_{15/2}$ at 1.53 μm is found to be higher than other reported phosphate glasses. The nearly broad and flat nature of 1.5 μm emission and the other most favorable optical properties suggest the possibility of using these materials for broadband optical amplification. Especially the moisture insensitivity, large Er^{3+} ion doping capability and ion-exchange compatible nature, are the most advantage features for short-length optical waveguide amplifiers, and such experiments are under progress.

Acknowledgements

The financial support from Department of Information Technology (DIT), Govt. of India, under Photonics Development Program (ref: 12(1)/2008-PDD) is gratefully acknowledged.

References

[1] Optical Technologies in Motion, European Commission's Information Society Technologies (IST-OPTIMIST), Fifth Framework (FP-5, 1998–2002) Projects (www.ist-optimist.org).
[2] (a) M. Yamada, M. Shimizu, Nippon Telegraph and Telephone Corporation (NTT) Tech. Rev. 1 (2003) 80–84;
(b) S. Aozasa, T. Sakamoto, H. Ono, A. Mori, M. Yamada, NTT Tech. Rev. 2 (2004) 44–49, www.ntt.co.jp.
[3] J.L. Wagener, C.W. Hodgson, M.J.F. Digonnet, H.J. Shaw, J. Light Wave Technol. 15 (1997) 1681–1688.
[4] X. Meng, J. Qiu, M. Peng, D. Chen, Q. Zhao, X. Jiang, C. Zhu, Opt. Express 13 (2005) 1628–1634.
[5] L. Huang, A. Jha, S. Shen, X. Liu, Opt. Express 12 (2004) 2429–2434.
[6] R.A. Martin, J.C. Knight, IEEE Photon Technol. Lett. 18 (2006) 574–576.
[7] W. Jin Chung, J. Choi, Y.G. Choi, J. Alloys Compd. 505 (2010) 661–667.
[8] K. Liu, E.Y.B. Pun, J. Alloys Compd. 470 (2009) 340–346.
[9] G. Vijaya Prakash, Mater. Lett. 46 (2000) 15–20.
[10] K. Pradeesh, C.J. Otton, V.K. Agotiya, M. Raghavendra, G. Vijaya Prakash, Opt. Mater. 31 (2008) 155–160.
[11] C.R. Mariappan, G. Govindaraj, S.V. Rathan, G. Vijaya Prakash, Mater. Sci. Eng. B 123 (2005) 63–68.
[12] (a) C.R. Mariappan, G. Govindaraj, S.V. Rathan, G. Vijaya Prakash, Mater. Sci. Eng. B 121 (2005) 2–8;
(b) G. Govindaraj, C.R. Mariappan, Solid State Ionics 147 (2002) 49–59.
[13] G. Vijaya Prakash, R. Jagannathan, Spectrochim. Acta A 55 (1999) 1799–1808.
[14] R.K. Brow, R.J. Kirkpatrick, G.L. Turner, J. Am. Ceram. Soc. 76 (1993) 919–928.

[15] G. Lakshminarayana, J. Qiu, M.G. Brik, G.A. Kumar, I.V. Kityk, J. Phys.: Condens. Matter 20 (2008) 375101–375108.
[16] V.A.G. Rivera, E.F. Chillcce, E. Rodriguez, C.L. Cesar, L.C. Barbosa, J. Non-Cryst. Solids 352 (2006) 363–367.
[17] R.N. Devi, K. Vidyasagar, Inorg. Chem. 39 (2000) 2391–2396.
[18] K. Subrahmanyam, M. Salagram, Opt. Mater. 15 (2000) 181–186.
[19] P. Gray, L.C. Klein, J. Non-Cryst. Solids 68 (1984) 75–86.
[20] W.D. Kingery, H.K. Bowen, D.R. Uhlmann, Introduction to Ceramics, Wiley, New York, 1976.
[21] S. Jiang, T. Luo, B. Hwang, F. Smekatala, K. Seneschal, J. Lucas, N. Peyghambarian, J. Non-Cryst. Solids 263 (2000) 364–368.
[22] A. Shaim, M.Et. tabirou, L. Montagne, G. Palavit, Mater. Res. Bull. 37 (2002) 2459–2466.
[23] H.S. Liu, T.S. Chin, S.W. Yung, Mater. Chem. Phys. 50 (1997) 1–10.
[24] B.R. Judd, Phys. Rev. 127 (1962) 750–761.
[25] G.S. Ofelt, J. Chem. Phys. 37 (1962) 511–520.
[26] H. Desirena, E.D. Rosa, L.A. Diaz-Torres, G.A. Kumar, Opt. Mater. 28 (2006) 560–568.
[27] P. Nandi, G. Jose, C. Jayakrishnan, S. Debbarma, K. Chalapathi, K. Alti, A.K. Dharmadhikari, J.A. Dharmadhikari, D. Mathur, Opt. Express 14 (2006) 12145–12150.
[28] L. Wetenkamp, G.F. West, H. Tobben, J. Non-Cryst. Solids 140 (1992) 35–40.
[29] P. Nachimuthu, R. Jagannathan, J. Am. Ceram. Soc. 82 (1999) 387–392.
[30] R. Reisfeld, C.K. Jorgensen, Lasers and Excited States of Rare-earths, Springer Verlag, NY, 1975.
[31] S. Tanabe, T. Ohyagi, N. Soga, T. Hanada, Phys. Rev. B 46 (1992) 3305–3310.
[32] C.C. Santos, I. Guedes, C.K. Loong, L.A. Boatner, A.L. Moura, M.T.D. Araujo, C. Jacinto, M.V.D. Vermelho, J. Phys. D: Appl. Phys. 43 (2010) 025102–025109.
[33] D.K. Sardar, J.B. Gruber, B. Zandi, J.A. Hutchinson, C.W. Trussell, J. Appl. Phys. 93 (2003) 2041–2046.
[34] A.J. Barbosa, F.A.D. Filho, L.J.Q. Maia, Y. Messaddeq, S.J.L. Ribeiro, R.R. Goncalves, J. Phys. Condens. Matter 20 (2008) 285224–285232.
[35] P. Babu, H.J. Seo, K.H. Jang, R. Balakrishnaiah, C.K. Jayasankar, K.S. Lim, V. Lavin, J. Opt. Soc. Am. B 24 (2007) 2218–2228.
[36] Y. Yan, A.J. Faber, H. de Waal, J. Non-Cryst. Solids 181 (1995) 283–290.
[37] X. Feng, S. Tanabe, T. Hanada, J. Non-Cryst. Solids 281 (2001) 48–54.
[38] J. Yang, S. Dai, Y. Zhou, J. Appl. Phys. 93 (2003) 977–983.
[39] M.J. Weber, D.C. Ziegler, C.A. Angell, J. Appl. Phys. 53 (1982) 4344–4350.
[40] H. Fan, G. Wang, K. Li, L. Hu, Solid State Commun. 150 (2010) 1101–1103.